On Data Scatter in Measured Linking Times for Lift-Generated Vortex Pairs

Vernon J. Rossow[*] and Larry A. Meyn[†]

NASA Ames Research Center, Moffett Field, CA 94035

The long-wave instability of a vortex pair spreads vortex wakes vertically and laterally faster than any other known aerodynamic mechanism. Initiated by turbulence in the atmosphere, the long-wave instability occurs frequently. However, measurements in flight of the timing of the process for a range of atmospheric turbulence levels contain a large amount of scatter around predicted values. Possible causes for data scatter are studied by use of a formulation for initiation and growth of the instability that differs slightly from Crow's and Sarpakaya's. It is concluded that some of the scatter may be due to the fact that the strength of vortex filaments in vortex pairs may sometimes be lower than the total centerline circulation on the wing, which causes the growth rate of the instability to be less than predicted. Another source for uncertainty may be caused by the way that the strength of the turbulence in the atmosphere was measured. Suggestions are made on how to use existing information to estimate the growth rate of the instability, and on how the turbulence in the atmosphere should be measured to achieve reliability.

Nomenclature

a = peak-to-peak amplitude of long-wave instability, ft (m)

A = a/b_g

b = wingspan, ft (m)

b' = spanwise distance between vortex centers $\approx \pi b_g/4$, ft (m)

B_{hz} = breadth of hazardous part of wake region to be avoided, ft (m)

C_L = lift coefficient = Lift/$q_\infty S$

C_l = rolling moment coefficient = Rolling moment/$q_\infty Sb$

D_{hz} = depth of hazardous part of wake region to be avoided, ft (m)

GPS = global positioning system

Kn = knots

G = $\Gamma/b_g U_\infty$

q_∞ = $\rho_\infty U_\infty^2/2$

S = planform area of wing, ft^2 (m^2)

t = time, s

T_g = $\tau\, G$

x = distance in flight or longitudinal direction, ft (m)

y, z = distance in lateral and vertical directions, ft (m)

u, v, w = velocity components in x, y and z directions, ft/s (m/s)

---

[*] Ames Associate, Aviation Systems Division, Mail Stop 210-10, AIAA Associate Fellow.
[†] Aerospace Engineer, Aerospace Modeling Office, Mail Stop 210-10, AIAA Associate Fellow.

U_∞ = velocity of wake-generating aircraft, ft/s (m/s)
Wt = weight, lbs (N)
Δt = time interval between wake-generating and following aircraft
ε = turbulence level
Γ **=** centerline circulation on wing, ft^2/sec (m^2/s)
θ = angle between vertical and plane of waves, degrees
ρ = air density, slugs/ft^3 (kg/m^3)
τ = time parameter = tU_∞/b_g

Subscripts
0 = initial value
decomp = decomposing wake
f = following aircraft
fil = vortex filament
g = wake-generating or leading aircraft
lnk = linking of vortex pair
lw = long-wave instability of vortex pair
max = maximum
min = minimum
oval = streamline oval that encloses vortex pair
pln = plan view
pr = vortex pair
t = turbulence
∞ = free-stream condition

I. Introduction

The hazard posed by lift-generated vortices inhibits the capacity of airports to accommodate landing and takeoff operations. The first solution tried was to separate runways by distances large enough that vortex wakes shed by leading aircraft would decompose to a harmless level before intruding into the airspace of other runways. As a consequence, runways could be operated independently from one another, but the land area required for additional runways to accommodate increasing traffic volume was difficult to obtain. Therefore, attempts were made to decrease the time between aircraft landing on the same runway. Such a procedure was impractical because the time intervals used to allow an aircraft wake to decompose to a harmless level was determined by aircraft size, wind and the turbulence in the atmosphere, which could not be changed.

An alternative method for increased capacity at airports was studied in the late 1960's and the 1970's. It considered the modification of the lifting surfaces on the wake-generating aircraft so that the vortices shed would decompose more rapidly.[1] The specific goal was to find those aerodynamic features of aircraft wings that would render lift-generated vortex wakes non-hazardous to following aircraft so that they could safely follow each other in-trail to the same runway within one minute or less. This goal was not achieved because all of the effective alleviation mechanisms discovered by the study also reduced the performance of the modified aircraft by an unacceptable amount.[1]

Another part of the foregoing research program was directed at finding effective and efficient ways to avoid the vortex wakes of preceding aircraft.[2-17] The present research effort does not attempt to reduce the in-trail time between aircraft landing on the same runway, because the increase[2-6] in airport capacity to be achieved is less than about 10%. In contrast, it is estimated that the capacity of airports can be safely increased by a factor of two or more by use of an improved wake-avoidance method for airport operations on sets of closely-spaced parallel runways.[7-17]

The technique being studied is an extension of current operations on closely-spaced parallel runways wherein operations are only conducted as nearly simultaneous landings during visual flight conditions. Encounters with vortex wakes are safely avoided because the along-trail spacing between aircraft landing on two closely-spaced parallel runways is intended to be so small that the vortex wake shed by either aircraft does not have time to spread enough to intrude into the airspace of the other aircraft, until after both have landed. Nearly simultaneous

approaches and landings require that the two aircraft have nearly the same approach and landing velocities. The extension being considered involves an increase in the along-trail separation distance or time for a pair of aircraft from nearly simultaneous to about 5 s (about 1000 ft or 305 m) to as much as 20 s (about 4000 ft or 1220 m). A variation in along-trail intervals between aircraft has a small effect on airport capacity, but it provides the ability to accommodate aircraft with different approach and landing velocities, which is a large advantage in the management of aircraft operations.

During visual-flight-rule conditions, two aircraft can land safely in concert on closely-spaced parallel runways. This is accomplished by the pilots of the two aircraft visually monitoring their longitudinal position relative to the other aircraft so as to remain in the safe zone, as shown in Fig. 1. When weather degrades to instrument conditions, only one of the two runways is used, which cuts the landing capacity in half. Efforts are underway to reliably and accurately predict this safe zone and to enable pilots to remain inside it during instrument conditions.

A challenge in reliably predicting the safe zone is that wake vortices transport and spread due to atmospheric turbulence and the long-wave, or Crow, instability. Measurement-scatter in the timing of the long-wave instability requires conservative predictions of the wake-hazard area, which reduces the safe zone by an amount that may not be necessary. The reduced safe zone restricts landing operations to aircraft pairs with similar approach speeds. The objective of the research presented here is to reliably increase the length of the safe zone by explaining possible physical reasons for the measurement scatter. Although the convection of vortex wakes by the wind can be reliably estimated, the transport and spread of elements of vortex wakes by turbulence in the ambient air, and by the long-wave (or Crow[18]) instability of a vortex pair presently have a high uncertainty.[19,20] The research presented here extends previous work by providing an explanation for the large amount of scatter in measurements of how fast vortex wakes are spread by the long-wave instability.

In the text to follow, some background information on the long-wave instability and some definitions of terms related to vortices are

Fig. 1 Safe and unsafe along-trail separation distances for following aircraft due to intrusion of wake shed by leading aircraft into its airspace.

first presented. The analysis then presents and discusses the data available on vortex linking times.[19-30] To explore the linking process by use of additional independent parameters, a velocity-based formulation for wake-spreading by the long-wave instability is derived and compared with flight data, with the theory of Crow and Bate[18-20] and with that of Sarpkaya[25-30] for a range of turbulence levels. It is found that both the circulation content assumed for the vortex filaments and the turbulence level in the atmosphere may need to be determined differently if a reliable representation of the dynamics of vortex pairs is to be achieved. Suggestions are then made on how to achieve conservative values for wake-spreading rates.

II. Background on Long-Wave Instability of a Vortex Pair.
A. Dynamics of Instability.

An example of a vortex pair undergoing the long-wave instability is presented in Fig. 2 by use of a sequence of photographs. The lift-generated vortices as marked by frozen exhaust condensate begin as relatively straight vortex filaments trailing from the aircraft wing as shown in the upper photograph. After a brief period of time, turbulence in the air where the vortices are embedded causes sinuous waves to form or to be initiated on the filaments. With the support of perturbation velocities in the turbulent flow field, and the self-induced velocity of the sinuous vortex pair, the waves eventually grow large enough to cause the two filaments to link at the troughs of the waves across the span to form irregularly-shaped vortex loops. The loops of vortices are noted in Fig. 2 to then spread vortex segments, and the wake hazard they present, even more rapidly. As a consequence, the instability has become known for its ability to decompose and spread vortex wakes more rapidly than any other known aerodynamic process.
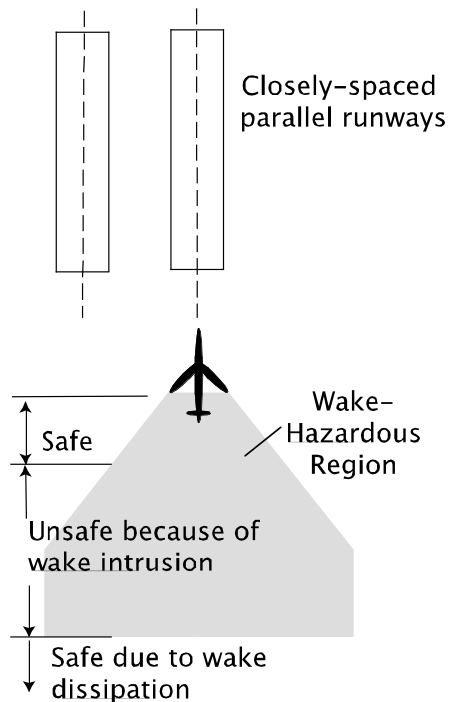
Extensive efforts have been made to understand the characteristics of the long-wave instability so that reliable predictions can be made of the decomposition and spread of vortex wakes. Safe and reliable separation distances between aircraft can then be estimated for the time available for safe along-trail separations between aircraft arriving for landings on closely-spaced parallel runways.[18-30] Because the rate of the spreading process increases rapidly after the vortex pair has linked to form irregularly-shaped loops (Fig. 2), linking is the event that is used as the end of the first "safe" region shown in Fig. 1. For this reason, prediction of the linking event is chosen as the critical event for nearly simultaneous landings on closely-spaced parallel runways.

If a reliable method can be developed for the prediction of the linking time of vortex pairs as a function of the turbulence level in the atmosphere, it is expected that efficiency and capacity of closely-spaced parallel runways can be increased, because landing operations can then be used with a wider variety of along-trail spacing between aircraft when needed. For example, at times when the atmosphere is quiescent, the hazardous regions associated with vortex wakes spread more slowly than when highly turbulent, so that the safe zone in Fig. 1 could vary from around ten seconds up to about a minute. However, when the turbulence intensity of the atmosphere is intense, it may be necessary to restrict the length of the safe zone to 10 s or less.
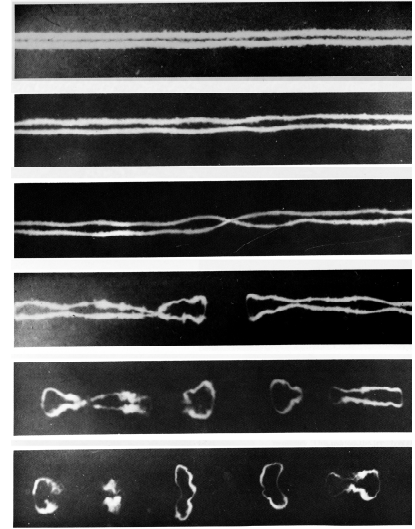

Fig. 2 Photographs taken at 15s intervals from below the condensation wake of a B-47 in cruise configuration to illustrate long-wave instability of a vortex pair; from Crow[18].

B. Definitions Associated With Vortices.

Several parameters to be used are defined next. It is well known that the circulation bound in the wake-generating wing rolls up into a vortex pair with centers near the wingtips (at about $y = \pm \pi b_g/8$). The magnitude of the circulation in each trailing vortex is then equal to the total circulation bound in the wing, Γ_{ac}, and no apparent indication is given in the flow field where the outer boundary of circulation ends. Inviscid theory indicates that the circulation is contained within a radius of $r = \pi b_g/8$. A vortex core is defined as the radius, r_c, at which the swirl velocity, which is a function of radius, is largest. The maximum diameter at which condensation is observed is sometimes used as a core diameter, but such is usually not the case. Instead, the appearance of condensation is related to the magnitude of the swirl velocity and the relative humidity in the air, and not to the maximum radius where condensate is visible.

A vortex filament is defined as a small-diameter line representation that approximates vortices that have their circulation spread over a diameter that may be as large as $\pi b_g/4$ or about 80% of the wingspan. In the linking process, it was assumed by Crow and Bate[19] that the circulation content of the filaments, Γ_{fil}, used in their analysis was the same as the total centerline circulation bound in the wing, Γ_{ac}. Such an assumption may not be the case, because observations[22,31-34] of condensation wakes of aircraft at cruise altitudes, and computations to be discussed, indicate that Γ_{fil} may be considerably less than Γ_{ac}. See discussion and photographs in the Appendix. The foregoing definitions will be used in the following analysis to explain the scatter observed in flight measurements as to the time at which vortex linking occurs as a function of the turbulence level in the atmosphere.

III. Data Available for Linking Times for Long-Wave Instability.

A. Flight Data.

The data available for the time interval between wake generation and when wake-vortex filaments link were obtained as part of research directed at the long-wave instability as a tool for wake decomposition. In some of the data, wake bursting may have been interpreted as wake destruction and treated the same as linking, which is a precursor of wake decomposition. Also, because no mention was made of wake division while making the observations, it is not certain whether the vortex filaments observed in the data-taking process contained all or only part of the total circulation shed by the aircraft. (see Appendix). The data points presented in Fig. 3 were read from figures in papers by Crow and Bate[19] and Tombach.[20] For comparison purposes, theoretical estimates developed by Crow and Bate[19] and by Sarpkaya[27] are shown as dashed lines in Fig. 3. The same log-log axes used in those papers are also used in Fig. 3 to retain the relationships established previously. The flight data are believed to be the only available for determination of a reliable time-to-linking relationship needed to define wake-spreading and

wake-intrusion times as a function of atmospheric turbulence. Unfortunately, the flight data in Fig. 3 scatters by a factor of 2 to 5 about the predicted values. In the theories and data presented in the figure, the self-induced downward velocity w_{pr}, is based on the initial vortex strength and separation distance estimated for each aircraft. The following analysis indicates that such an assumption may be in considerable error, and thereby causing some of the scatter in the vertical direction. Scatter in the horizontal direction is believed to be caused by the way that the magnitude of the disturbance velocities were determined for initiation of the long-wave instability.

B. Water Tow-Tank Data.

The data points obtained in water tow tanks[23-30] are not shown in Fig. 3 because their large number obscures the two theoretical curves and the flight data that are the preferred reference quantities to be used here. The extended Crow-Bate theory developed by Sarpkaya[25-27] is shown in Fig. 3 because it provides an approximate average of all of the tow-tank data. Sarpkaya's recommended curve is about the same shape, but it is above the curve predicted by the theory of Crow and Bate.[19] Data taken by Liu[24] is best approximated by the Crow and Bate curve. The data obtained by Delisi[29] in a water tow tank are in good agreement with Sarpkaya's curve. Even though the tow-

Fig. 3 Comparison of prediction methods of Crow and Bate[19] and of Sarpkaya[27] with flight data from Crow and Bate[19] and from Tombach[20] to indicate amount of scatter in measured data.

tank data are not in exact agreement with the theoretical predictions of Crow and Bate, it confirms the predicted trends and indicates that proper measurement of the flow-field parameters in the development of the long-wave instability does produce data that has a small amount of scatter.

The applicability of the three sets of data taken in water-tow tanks to subsonic transport aircraft is questioned because they were obtained with wake-generating wings of rectangular plan form that had an aspect ratio of around two. Those wings do not closely approximate those of current subsonic transport aircraft. It is to be noted that the scatter between the various ground-based facilities is small compared with the scatter of the flight data. The quality of the tow-tank data shows care, because the time-to-linking data obtained in tow tanks is consistent for a given grid or mesh size used to produce the turbulence in the tow tank.

A negative aspect of the data is that it appears to have a systematic change in the level of linking times when different sizes of turbulence-generating grids are used.[29] In addition, the largest grid size used in the various tow tanks is only large enough to produce turbulence eddies of wavelength sizes up to about 4b',[18,19] whereas the optimum wavelength for stimulation and support of the instability is 8.6b'. The extended Crow-Bate theory developed by Sarpkaya was developed to better simulate the effect of disturbance wave lengths on linking time. The intended greater applicability of Sarpkaya's theory may then represent the smaller wave length range generated by the grids. It may be possible that the tow tank results do not then produce complete turbulence spectrums that extend across the wave lengths needed for linking, and as expected in the atmosphere. For this reason, it seems that the measured time-to-linking curves might yield lower values for linking times if proper grid sizes are used, and thereby become in better agreement with the predictions of Crow and Bate.[19,23-29]

It was not possible to employ larger mesh sizes in the tow-tank tests, because the dimensions of the cross section of the facilities would not accommodate them. Even so, the experiments demonstrate that data quality for linking times can be good when experimental parameters are tightly controlled, and measured accurately. It is concluded that, although the data obtained in the ground-based facilities contribute substantially to the understanding of the dynamics of the long-wave instability and linking of vortex pairs, it may be slightly in error for the time-to-linking quantity in the atmosphere for vortex wakes produced by the high aspect-ratio wings now used on subsonic transport aircraft.

It is believed that the small amount of scatter in the water tow tank data is primarily due to the fact that the self-induced downward velocity of the vortex pair, w_{pr}, was measured directly rather than assumed to be the same as when the vortex wake was first generated. A direct measurement of the self-induced downward velocity of the vortex pair could be made in the water tow tank tests, whereas it is not readily measured in flight. As a consequence, the actual value for the self-induced downward velocity of the vortex pair, w_{pr}, can be used in the
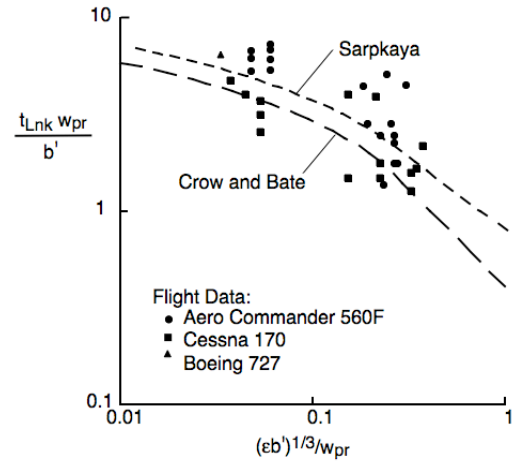
computation for each data point. Similarly, the turbulence level in the ambient fluid at frequencies that initiate the long-wave instability could be more readily measured in the tow tank than in the atmosphere. This was the procedure used by Delisi[29] to calculated the dimensionless parameters for the data shown in his paper. Therefore, it is believed that the scatter in the flight data is brought about by measurement techniques rather than by gross errors in the theoretical development.

Another quantity or parameter that may be causing scatter in the flight data is the assumption that the wave-number spectrum of the turbulence present in the atmosphere may not be as close to a Kolmogorov type[35-36] as assumed in the analysis.[18-29] If so, the method used to determine the turbulence level, or ε^*, for the various data points may be responsible for some of the scatter. That is, the magnitude of the perturbation velocities that initiate and support the long-wave instability was determined by use of a technique that may be unreliable. If so, it is suggested that the disturbance velocities in the flow field should be measured directly over the wavelength range most influential in initiation of the long-wave instability; i. e., about 4 b_g to 10 b_g. The optimum wavelength for initiation of the long-wave instability was found by Crow[18] to be 8.6 b' or about 6.8 b_g.

IV. Velocity-Based Formulation for Long-Wave Instability.
A. Self-Induced Growth Rate.

Crow[18] was the first to associate turbulence in the atmosphere with the initiation of waves on vortex pairs that trail from aircraft at cruise altitudes. He was also the first to relate the self-induced velocity field of the sinuous vortex filaments to the augmentation of the input from turbulent eddies into the amplification of the nearly sinusoidal waves on the vortex-filament pair. The self-induced velocity field of the sinuous shape of vortex filaments also provides a sorting mechanism that supports turbulence wavelengths only between about 4b' (b' = distance between centroids of vorticity $\approx \pi b_g/4$), and about 10 b', with the optimum wavelength at 8.6b' (i.e., $\approx$6.8 b_g). As a consequence, only the waves on the vortex filaments whose lengths are in this range are amplified by the velocity field of turbulence-initiated displacements of the vortex filaments. As a result, when properly stimulated by turbulence, the instability produces a set of sinusoidally-shaped waves from about 4b' to 10b' in length that grow rapidly in amplitude. Crow determined that the optimum turbulence wavelength for initiating the instability is 8.6b', and that the waves on the two vortex filaments must be nearly in phase to bring about the large-scale wake spreading and across-centerline linking of the vortices.[19,21] Therefore, only the in-phase case will be analyzed here, because it produces the most rapid wake-spreading rate.

Development of an empirical estimate for the rate of growth of the wave amplitude as a function of time begins with the use of numerical results derived previously.[21] The numerical data used to develop a numerical representation for the growth rate for the long-wave instability cases shown in Figs. 4-6 were calculated for a wave length of 6 b'. The vortex filaments have been given an initial peak-to-peak amplitude, a_i, of a given magnitude to study how the growth rate of sinusoidal waves responds to different initial amplitudes.[21] Because the numerical simulation is not able to represent the linking part of the long-wave instability the computation were stopped when the amplitude of the wave troughs began to grow rapidly. In the present model, the simulation of possible changes in the circulation content of the vortices is not considered, because it is uncertain as to the
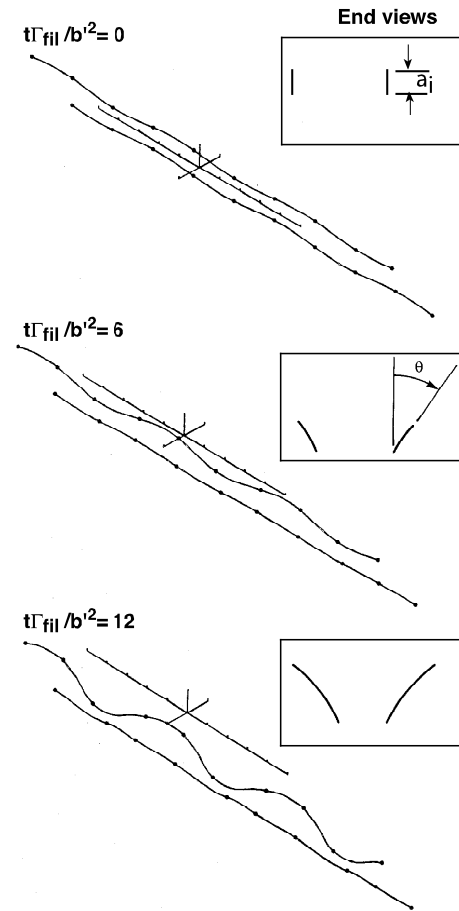

Fig. 4 Oblique and end views[21] of vortex pair which has an initial displacement of sine waves that are in phase to simulate long-wave instability; wavelength=6b', a_i = initial amplitude = 0.23b'.

mechanism by which the wake would divide in a way implied by the photographs presented in the Appendix.

As indicated in Fig. 4, along with the rapid growth of wave amplitude for in-phase waves on the vortex filaments, the two planes of oscillation of the waves on the two vortex filaments each rotate in a direction opposite to the rotation direction of the vortices themselves. When the amplitude of the waves has grown large enough, and the planes of oscillations have rotated through an angle, θ, to about 45° to 48° from the vertical, the vortices usually link across the wake centerline to form irregularly-shaped loops of vortex filaments (Fig. 2). After the vortices link, the loops of vortex filaments spread even more rapidly in both the lateral and vertical directions. In fact, once initiated, the amplitude of the waves grows exponentially.

The results for wave amplitude as a function of time from six numerically-produced cases like the one shown in Fig. 4 are summarized in Fig. 5 as a beginning step towards a representative equation for wave growth as a function of time. The curves presented in Fig. 5 provide numerical values for wave amplitude as a function of the time parameter, $t\Gamma_{fil}/b'^2$. The study did not cover how various eddy sizes and orientations, likely to occur in a turbulent flow field, were sorted out by the instability. It appears that the self-induced dynamics of the long-wave instability discards other turbulence-induced disturbances to form a relatively pure set of sine waves that persist and amplify. Conversely, when the disturbances necessary for growth of the long-wave instability are not present, sinuous waves do not occur, and vortex wakes decompose due to mechanisms other than the long-wave instability.

Fig. 5 Growth of peak-to-peak amplitude of long-wavelength instability as a function of time for several starting wave amplitudes.

C. Equations for Growth of Long-Wave Instability.

Because numerical instabilities limit long-term calculations of the self-induced growth of the long-wave instability (Figs. 4 and 5), a case analyzing growth from a small initial amplitude to the point of vortex linking could not be carried out. It was decided, therefore, to combine the results in Fig. 5 into a single curve that could be used to represent growth from very small disturbances up to the maximum amplitudes observed in experiments. The development of such a relationship began by shifting each of the curves in Fig. 5 by an increment in time so that the most rapid-growth parts of the various curves would align and overlap to form a single curve as shown in Fig. 6. It is argued that the initial parts of the curves, which protrude from the blended curve in Fig. 6, occur because the initial sinusoidal input given to each filament requires an adjustment period before the regular, rapid-growth process gets underway. If this initial adjustment process is ignored, and only the growth part of wave amplitude is accepted, all of the curves lay close to a single line. The solid curve in Fig. 6, which is a best visible fit to the data, is given by,

$$a_{lw}/b' = 0.06081 \exp(0.0178T_g^{1.5}) \qquad (4)$$

where, a_{lw} is the peak-to-peak wave amplitude, and $T_g = t\Gamma_{fil}/b'^2$, is a circulation-based time parameter for the long-wave instability. When T_g is zero, the wave amplitude is small but finite, and it is a function of the smallest
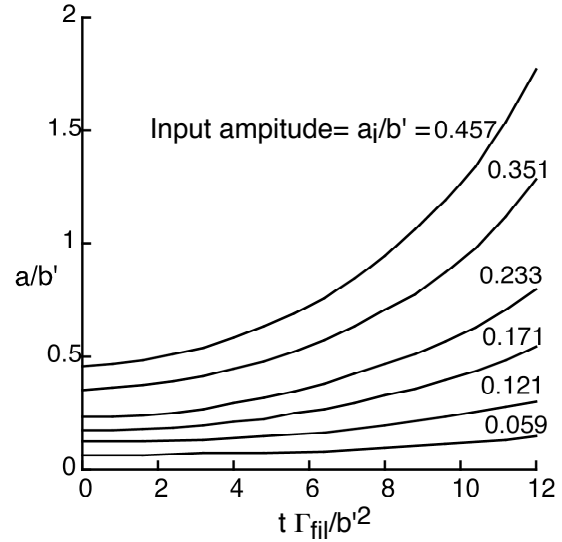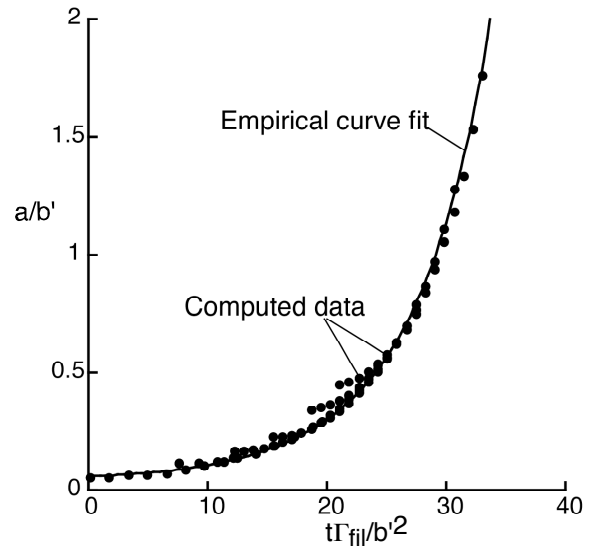

Fig. 6 Comparison of single empirical curve for amplitude of waves in long-wave instability as a function of time, with time-shifted data curves from Fig. 5.

input amplitude used in the numerical cases for Fig. 5, which is believed to be adequately small. Because negative values of time are required in Eq. (4) to achieve smaller amplitudes, and T_g is raised to the 3/2 power, values of amplitude below those given by $T_g = 0$ are not defined. Also note that Figs. 4-6 and the parameter, T_g, are based on the span-wise distance between the vortex centers, b', and not on b_g. Since the two quantities are usually related to each other by b' $\approx \pi b_g/4$, a form more applicable for use in practice is obtained by writing T_g in terms of b_g, rather than b', as

$$T_g = t\Gamma_{fil}/b'^2 = (4/\pi)^2(\Gamma_{fil}/b_g U_\infty)(tU_\infty/b_g) = 1.62114\, G_{fil}\,\tau \qquad (5)$$

The quantity, $G_{fil} = \Gamma_{fil}/b_g U_\infty$, is a circulation parameter that is assumed to be constant during any one instability event, and $\tau = tU_\infty/b_g$, is a dimensionless time parameter that relates time and distance during the event. The constants in Eq. (4) then change to

$$a_{lw}/b_g = 0.06081(\pi/4)\exp[0.0178(4/\pi)^3 G_{fil}^{1.5}\tau^{1.5}] \qquad (6a)$$

or,

$$a_{lw}/b_g = 0.04776\exp[0.03674 G_{fil}^{1.5}\tau^{1.5}] \qquad (6b)$$

Either Eq. (6a) or Eq. (6b) can be used to relate the peak-to-peak amplitude of the waves at one time to the amplitude of the waves at another time. Both equations predict the growth in amplitude of a set of input sinusoidal waves that have been placed on a pair of vortex filaments by turbulence. The equations also indicate that the larger the amplitude of the input waves, the faster they will grow, and therefore, a larger value of turbulence level will make the waves become even larger more quickly. Both of these characteristics are in agreement with the characteristics observed for the long-wave instability both in flight and in ground-based facilities.[18-29]

D. Initiation of Long-Wave Instability by Turbulence.

The following text discusses how the turbulence in the flow field where the vortex filaments are embedded initiates the long-wave instability of a vortex pair. Three sources of turbulence are usually present. The turbulence that resides in the atmosphere along the flight path of the aircraft is the first source of turbulence, and is important because it provides disturbances to the vortex pair over the wide range of frequencies and wavelengths needed for initiation of the instability. The second source is produced by the flow field around the aircraft, which is enhanced when flaps and/or landing gear are extended. It is believed that the turbulence shed by the flow over the aircraft does not contribute to initiation of the long-wave instability because most of its energy is at wavelengths smaller than the wingspan of the generating aircraft, which is too small to initiate the instability. The third source is the propulsion system, which contains energy over a wide range of frequencies as the energized flow field of the propulsive system ages. This source of turbulence for initiation of the long-wave instability is important at cruise altitudes, because, at those altitudes and along those flight paths, atmospheric turbulence is not generally present at sufficient intensities to initiate the instability. Because across-trail displacements of vortex segments by these sources of 'ambient' turbulence are what initiates the long-wave instability,[19] the relationship between vortex meander, initiation of the long-wave instability, and linking of a vortex pair are discussed.

It is first noted that during approach to a runway all three sources of turbulences may contribute to the initiation of the instability, but turbulence that exists in the atmosphere is probably the primary source of disturbances because engines are throttled down. Therefore, the parameter, ε_{max}, is used to quantify the intensity of random turbulent motions as,[10]

$$\varepsilon_{max} \approx |v'|_{max}/U_\infty \approx |w'|_{max}/U_\infty \qquad (7)$$

The parameter, ε_{max}, is the value of the maximum turbulence velocities measured in the atmosphere along the flight path of the wake-generating aircraft. The wavelengths of the disturbances of interest range from about 4b'$_g$ ($\approx$3.14 b_g) to beyond 8.6b'$_g$ ($\approx$6.8b_g), where the maximum amplification rate is predicted to occur.[18,19] Because the wavelengths of turbulence eddies that are effective at initiating and supporting the instability do not have a sharp cutoff, but fade away, it is recommended that the maximum values of |v'| and |w'| be measured in the wavelength

range from about $2b_g$ to $10b_g$ for the determination of the parameter ε_{max} to be certain that the entire effective wavelength range (and especially the maximum growth rate region of the instability) is covered. It is imperative that the maximum perturbation velocities be found, because those values represent the fastest possible growth rate of the instability waves. Therefore, they govern the earliest times at which hazardous elements of the wake intrude into the runway and airspace of following aircraft. The more reliably that the earliest occurrence of wake intrusion can be predicted, the more reliable is the level of safety. It is recommended that these velocity perturbations be measured with instrumentation on board the wake-generating aircraft so that measurements are taken in the same air space as where the vortices are embedded.

Note that the parameter ε_{max} is similar to the parameter used for the turbulence level to quantify the non-uniformity of wind-tunnel airstreams, as given by[37]

$$\varepsilon_t = [(\overline{u}'^2 + \overline{v}'^2 + \overline{w}'^2)/3U_\infty^2]^{1/2} \tag{8}$$

where ε_t is the root-mean-squared (rms) turbulence level in the flow field compared with the time-averaged free-stream velocity. The three primed and barred quantities inside the circular brackets represent the time-averaged values of the square of the three components of the measured perturbation velocities in the empty wind-tunnel air stream. Eq. (8) reduces to Eq. (7) when the measurements are restricted to the maximum perturbation values of either of the two velocity components perpendicular to the flight path of the wake-generating aircraft.

The foregoing definitions were found to be necessary because a lack of agreement existed between measured turbulence level and the maximum vortex meander distance in the two large wind tunnels at NASA Ames Research Center. Both facilities have a measured turbulence level of about, $\varepsilon_t = 0.005$.[38,39] If the across-vortex displacements of the vortex centers move exactly with the fluid, maximum meander distances should be closely related to the maximum disturbance velocities. Or, as a minimum, the maximum meander distances should be comparable with the measured rms turbulence level. However, this proved not to be the case. Instead, it was found that maximum measured meander distances yield a value of only: $\varepsilon_{meand} = |\overline{v}'|/U_\infty \approx |\overline{w}'|/U_\infty \approx 2/(12 \times 81) \approx 0.002$, which is 40% of the measured rms turbulence level. Also, the meander distances increased linearly with downstream distance in the wind tunnel. Although ε_{meand} is of the same order of magnitude as the $\varepsilon_t = 0.005$ level measured for the rms turbulence level in the free stream, it is not clear how the difference between the two should be reconciled.[13]

The difference between the two values of turbulence level may be caused by the fact that the vortices observed in the wind tunnel are not filaments, but have vorticity distributed over a radial distance of about $\pi b_g/8$. Displacement of the vortices may then be reduced by the inertia of the air involved,[13] and/or by the fact that the swirl velocities of fluid in the eddies involved may decay rapidly enough to cause measured differences. Whatever the reason for their difference, the lack of understanding and the desire for conservatism recommended that the measurements of maximum vertical and lateral disturbance velocities in the free stream, Eq. (7), be used to evaluate ε_{max}, which is defined as the maximum magnitude of the disturbance associated with the turbulence in the ambient fluid that drives the initiation of the long-wave instability.

V. Development of Equations for Wake-Spreading Rate
A. Equations for Growth of Long-Wave Instability.

The previous equations for the self-induced and the turbulence contributions to wave growth can now be combined for relationships that predict the amplitude of the waves formed on vortex filaments by means of the long-wave instability. The analysis begins with Eq. (6b) written as

$$d(a_{lw}/b_g)/d\tau = 0.055112(G_{fil}^{1.5}\tau^{1/2})(a_{lw}/b_g) \tag{9}$$

The parameter, $\tau = tU_\infty/b_g$, in Eq. (9) is a relative time quantity that must be eliminated before it can be combined with the contribution to wake spreading caused by turbulence-induced vortex meander; Eq. (7). From Eq. (6b),

$$\tau^{1/2} = [\ln(A_{lw}/0.4776)]^{1/3}/\{[0.03674]^{1/3}G_{fil}^{1/2}\} \tag{10}$$

where $A_{lw} = a_{lw}/b_g$, is the dimensionless form of the amplitude of the waves. After the quantity τ has been eliminated from Eq. (9), the differential equation for the self-induced wave growth rate becomes a function of wave amplitude only. The equation for the rate of self-induced amplitude growth then becomes only a function of wave amplitude and circulation content of the filaments as,

$$dA_{lw}/d\tau = 0.16579G_{fil}A_{lw}[\ln(A_{lw}/0.04776)]^{1/3} \tag{11}$$

which is usable, but is not of a form that can be integrated for a relationship between wave amplitude and time.

The quantity desired for wake spreading is a combination of the self-induced and turbulence-induced velocity contributions to the lateral spreading of the wake due to the long-wave instability. The differential equation is found by use of a combination of Eq. (11) for the self-induced contribution, and Eq. (7) for the contribution due to turbulence in the ambient stream as

$$dA_{pln} = [(dA_{lw}/d\tau)/2^{1/2} + 2\varepsilon_{max}] \, d\tau \qquad (12)$$

which is a function of time, the circulation content of the vortex filaments, G_{fil}, and the maximum magnitude of turbulence disturbances, ε_{max}, of the atmosphere where the vortices are embedded. Eq. (12) is therefore more complex than the solutions provided by Crow and Bate[19] and by Sarpkaya,[27,28] and cannot be integrated for a closed-form result. The quantity $1/2^{1/2}$ in Eq. (12) comes about because the plan view and not slant amplitude of the waves is needed for wake spreading. The quantity, A_{pln}, includes the contributions of both the turbulence in the air where the vortices are embedded, and the long-wave instability, $dA_{lw}/d\tau$. The turbulence term, $2\varepsilon_{max}$, does not need to be adjusted by a factor of $1/2^{1/2}$ because the spreading due to vortex meander as brought about by turbulence is assumed to spread vortex elements equally in all directions, whereas the long-wave instability spreads vortex elements only along a diagonal plane at about 45° to the horizontal. The present analysis ignores variations in the angle of the plane of the sinusoidal waves as a function of time, and assumes that they can all be approximated by an angle, θ, of about 45° to the horizontal.

In the numerical integration of Eq. (12), the first term that represents the influence of the long-wave instability is set equal to zero until its magnitude yields a positive contribution to wave growth; i.e., until $A_{lw}>0.04776$. Until then, the amplitude of the waves in plan view increases only due to the contributions of the turbulent part of the flow field. Unreal values of wave growth are then avoided during the starting part of the instability, where the wave amplitude is small.

Because half of the wave extends inboard from its undisturbed location, and half extends outboard, the vortices link when the amount of spread in the wake-hazardous breadth becomes $b'=\pi b_g/4$ for the total amount and, $\pi b_g/8=0.3927b_g$ on each side of the wake. Although not used for amplitudes larger than linking, wake spreading is still represented by Eq. (12) because the empirical wave-growth equation is based on data all the way to maximum amplitude. At maximum amplitude, the maximum total distance between relocated vortex centers is about 5b'; e.g., Fig. 2. Because the original separation distance between vortex centers is equal to b', the span-wise increase is 4b', which means that each side of the wake has increased by 2b' (or $\pi b_g/2$) at the estimated maximum amplitude of the long-wave instability. After linking, the self-induced velocity field of the irregularly-shaped loops of vortex filaments cause wake elements to continue to spread. Because the empirical equations for amplitude growth are based on growth beyond linking, the equations should also predict about the correct wake-spreading rate out to maximum vortex separation distances of 5 b' or greater. The separate contributions due to turbulence and to the self-induced velocity field of the filaments are illustrated in Fig. 1 by the dashed lines and the solid lines respectively.

Before leaving this derivation, another feature of flexibility is added to Eq. (12). The necessity for the addition came about when it was found that the use of ε_{max} as constant with time probably over estimates the effectiveness of turbulence eddies in their initiation of the long-wave instability and in the support of wave growth thereafter. Addition of an expression that models the exponential decay of turbulent eddies permits study of possible changes in the strength of the driving eddies during the development of the long-wave instability. It will be seen in the next section that variations in eddy strength are needed if delayed linking in some flight cases is to be represented. Therefore, the continuous support of growth of the long-wave instability by use of a constant value of ε_{max} was modified by allowing the input of turbulence to have an exponential decay rate. Such a variation appeared reasonable, because observations of smoke-marked eddies in the atmosphere during the NASA wake-vortex program of the 1970s indicate that rapid rotations of fluid does appear to slow a great deal during their first cycle of swirl.[1] As a consequence, Eq. (12) is rewritten as,

$$dA_{pln} = [(dA_{lw}/d\tau)/2^{1/2} + 2\varepsilon_{max} \, e^{k\tau}] \, d\tau \qquad (13a)$$

This empirical equation makes it possible to analyze the long-wavelength phase of vortex filaments as affected by a decaying turbulent eddy, rather than by a steady-state eddy. The parameter, k, is assumed to be of the form

$$k = \varepsilon_{max} (b_g/\pi\lambda) \qquad (13b)$$

Approximate decay estimates for the eddies were used to test experimental data points to find out if decay of swirl velocities helps to explain the scatter observed. It is unlikely that measurements can or will be made of the decay parameter in operational situations, even though the physical process is present.

A much simpler equation was derived by Crow and Bate[19] for the case when the turbulence level is so high that it dominates the self-induced velocity field of the vortex-filament pair. A similar relationship is now derived from the present analysis. Under those circumstances, Eq. (12) simplifies to

$$dA_{pln} \approx [2\varepsilon_{max}]\, d\tau \tag{14a}$$

which can be integrated from the time when the filaments were first generated to when they link to yield
$A_{pln} = 2\varepsilon_{max}\, \tau_{Lnk} = b'/b_g$ which makes it possible to write the linking time as

$$\tau_{Lnk} = (\pi/8)/\varepsilon_{max} = 0.3927/\varepsilon_{max} \tag{14b}$$

If it is assumed that $|v'_{max}| \approx |w'_{max}| \approx (\varepsilon b')^{1/3}$. Eq. (14b) is in good agreement with the value of 0.41 given by Crow and Bate for their strong turbulence case when the values for the turbulence level for the two theories are the same. In practice, ε_{max} will always be larger than the values used by Crow and Bate because it is based on maximum values of disturbance velocities, whereas their values are based on root-mean-squared values, which are less conservative, but better represent situations for complete wake decomposition.

B. Conversion of Nomenclature.

The parameters introduced by Crow and Bate[19] originate with their solution method, and were used by others[23-30] to study the long-wave instability. The parameters they used to make the atmospheric turbulence and the time-to-linking parameters into dimensionless form are, b', the initial lateral spacing between the two vortex filaments, and the theoretical initial descent velocity of the vortex pair as given by

$$w_{pr} = \Gamma_{ac}/2\pi b' \tag{15a}$$

which is related to G_{ac} and U_∞ by

$$w_{pr}/U_\infty = (\Gamma_{ac}/b_g U_\infty)(b_g/2\pi b') \approx (2/\pi^2)G_{ac} \approx 0.2026 G_{ac} \tag{15b}$$

where $b_g/b' \approx 4/\pi$, and Γ_{ac} is the centerline circulation bound in the wake-generating wing. In the present analysis, the flight velocity of the wake-generating aircraft, U_∞, is used as the reference velocity, rather than w_{pr}. In order to compare the predicted values by the two theories, it is assumed for comparison purposes only that the magnitude of the disturbance velocities that initiate the long-wave instability are of the same magnitude in both notations, or that

$$|v'_{max}| \approx |w'_{max}| \approx (\varepsilon b')^{1/3} \tag{16}$$

Such will actually not be the case, because $|v'_{max}|$ and $|w'_{max}|$ are the maximum disturbance velocities measured in the vicinity of the vortex pairs, and $(\varepsilon b')^{1/3}$ is based on a root-mean squared value. Because a definitive ratio between the maximum disturbance velocities and the one based on the eddy-dissipation rate is not available, it will be assumed that they are equal for the comparisons to be made of the two theories. A definitive set of data is needed to define the relationship of linking time to the type of measurement used to determine the disturbance velocity. An average value for the conversion of one set of dimensionless parameters to the other for the ratio, w_{pr}/U_∞, is found by use of two equations for the lift on the wake-generating aircraft in the form

$$\text{Lift} = \text{aircraft weight} = \rho b' U_\infty \Gamma_{ac} = C_{Lg}(\rho U_\infty^2/2)\, b_g^2/AR_g \tag{17a}$$

which leads to,

$$\Gamma_{ac}/b_g U_\infty = (C_{Lg}/2AR_g)(b_g/b') \tag{17b}$$

An average value for the vortex descent velocity for subsonic transport aircraft is then related to the free stream velocity by,

$$w_{pr}/U_\infty)_{ave} = C_{Lg}(b_g/b')^2/(4\pi AR_g) \approx 0.0276 \tag{17c}$$

when $C_{Lg} \approx 1.5$ and $AR_g \approx 7$, which approximate subsonic transport aircraft.

Because the initial circulation content in the vortex pair, $G_{ac} = \Gamma_{ac}/b_gU_\infty$, may not be the same as the circulation content of each vortex in the pair during the dynamics of the long-wave instability, the value of the dynamics of vortex filaments during the long-wave instability will be represented by $G_{fil} = \Gamma_{fil}/b_gU_\infty$. For vortex filaments, the self-induced downward velocity of vortex filaments is then given by

$$w_{pr})_{fil} = \Gamma_{fil}/2\pi b' \qquad (17d)$$

The various parameters used by Crow and Bate, and others, can now be related to those used in the present analysis (and which are suggested for use in operational situations).

III. Results of Computations.
A. Comparisons of Theories With Each Other and With Experiment.

In Fig. 7, the velocity-based predictions of dimensionless linking times are compared with the same information presented in Fig. 3. The vertical axis is expanded one decade and the horizontal axis by two decades to better indicate the nature of the curves at extreme values of the parameters. The three theories are shown on the same figure because, the velocity-based predictions are adjusted to the Crow-Bate and Sarpkaya nomenclature by use of Eq.(15b) for the ratio w_{pr}/U_∞, and for the fact that $b_g/b' \approx 4/\pi$. As indicated by Eq. (16), the magnitude of the disturbance velocities used in the predictions are assumed to be of the same magnitude in this comparison so that the differences in the curves are restricted to the theoretical treatments used in the derivations. That is, it is assumed

that, for comparison of the three theories, $|v'_{max}| \approx |w'_{max}| \approx (\varepsilon b')^{1/3}$. When applied to actual turbulent flow fields, the three parameters will no doubt have different magnitudes of disturbance velocity, which will yield different linking times for differing purposes. For example, use of $(\varepsilon b')^{1/3}$ for the disturbance velocity will yield an estimate of root-mean-squared linking time for wake-dissipation estimates. Similarly, use of $|v'_{max}|$ or $|w'_{max}|$ will yield a stronger value for the turbulence level, and therefore the shortest linking time for use as estimates of wake-intrusion times into adjacent runways. Therefore, in practice, the two measured disturbance levels will usually differ considerably.

Although the derivation process used to obtain the various theoretical predictions are different, the curves in Fig. 7 are close to each other over the parameter range displayed. In plotting the velocity-based predictions, it was found that the single curve shown for the velocity-based prediction is composed of a series of smaller curves for separate values of G_{fil} that

Fig. 7 Comparison of velocity-based predictions, Eq. (12) in terms of Crow-Bate nomenclature with two previous theories and flight data.

overlap to form a single curve across the entire parameter space. It is also noted that, at small values of disturbance velocities, the velocity-based theory indicates that the time to linking is going to infinity, which conforms with the nature of the process.

B. Simulation of Wake Division.

Velocity-based predictions are now used to explore the possibility that the flight-data points are not properly located on the graphs because of wake-division (see Appendix). Because enough information is not available to relocate the data points on the graph, they are left as presented by Crow and Bate. Instead, the versatility of the velocity-based predictions are used to simulate different values of circulation G_{fil} in the filaments, for a given value of w_{pr} to explore the amount of reduction in circulation required for an explanation of the scatter in the data points. The points shown in Fig. 7 for the flight data assume that the full initial circulation shed by the wake-generating wing stays with the vortex filaments throughout the long-wave instability event. Therefore, the parameters in the velocity-based equations need to be adjusted for w_{pr} by use of an estimated average value of the assumed circulation in the filaments given in Eq. (17c) for $w_{pr}/U_\infty)_{ave}$. An estimated circulation content that might have existed in the
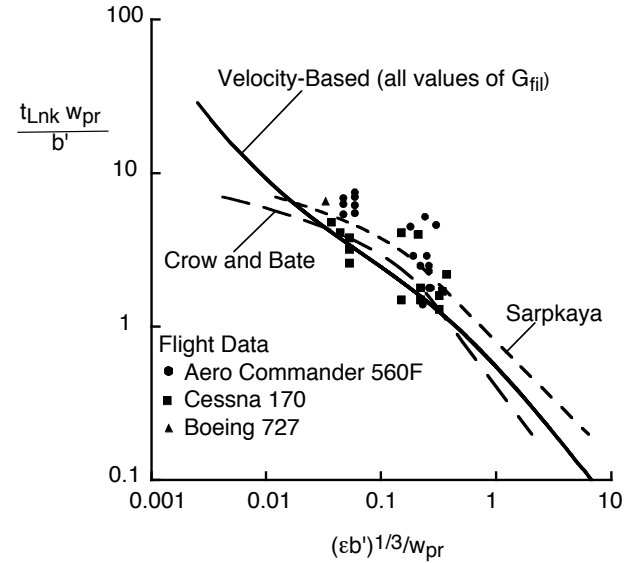
flight experiments is then represented by a value for G_{fil} as indicated for each of the curves in Fig. 8. The separate curves for various values of G_{fil} then no longer fall on a single curve, but form a series of curves. These results indicate that, if the actual circulation in the vortex filaments during the flight experiment is not the same as assumed in data-reduction process, the data points will be located at larger values of linking time as the circulation content of the filaments shrinks.

The simulated wake-division process with the velocity-based formulation suggests that at least some of the scatter in the flight data is a result of improper values for the circulation content, G_{fil}, assigned to the vortex filaments in the data-reduction process. That is, the circulation content assumed was G_{ac} , and the value that should have been used is G_{fil}.

A shortcoming in the representations presented in Fig. 8 exists on the right side of the graph where the simulated curves fall below the flight data. A possible reason for the failure of the simulation in that part of the graph was discussed just after the derivation of the velocity-based equations. It was reasoned that the assumption of a constant strength for the turbulent eddy

Fig. 8 Simulation of reduced circulation content in vortex filaments by use of velocity-based theory to explain some of scatter in flight data.

that is driving the sinuous waves on the filaments may overstate the persistence of the magnitude of the disturbance velocity. To explore such a possibility, several values of exponential decay for the eddy velocity in Eq. (13) were tried to determine if a value for decay rate would improve agreement between the predicted and measured data. On the basis of the flight data located in the upper right of Fig. 8, it was estimated that a value of 50 for the parameter, k, in Eq. (13), is best suited for a match with the flight data. Comparisons presented in Fig. 9 indicate that decay of

the turbulent eddies is then better able to account for all of the scatter above the theoretical curves that was observed in the experimental data.

Typical values of bound circulation for subsonic transports are around $G_{ac} = 0.14$ during approach and landing, and around $G_{ac} = 0.10$ when at cruise altitudes. The comparisons in Fig. 7 indicate that the velocity-based and the Crow and Bate theories are roughly in agreement for those values of G_{fil} over mid-range values of turbulence level, where $G_{fil} \approx G_{ac}$. The predictions of the two theories have about the same overall slope, but the curvatures of the predicted values on a log-log scale for the two theories are quite different when plotted on logarithmic scales.

Fig. 8 and 9 also indicates that, because of scatter in the flight data, values of G_{fil} needed for agreement between experiment and the present theory require values of G_{fil} as low as about 0.014 and as high as about 0.3. However, subsonic jet transports usually do not have values of G_{fil} of 0.20 and higher. Values in the upper range are associated with powered-lift aircraft. As explained in the Appendix, values of circulation content of the filaments in the low range

Fig. 9 Comparison of velocity-based theory for decaying eddies, k = 50 in Eq. (13), with flight data and with theories of Crow and Bate,[19] and Sarpkaya,[27] in their notation.

may be provided by recognition that lift-generated vortices have been observed to divide into two vortex-like regions. Division of vortices could lead to vortex filaments with low values of concentrated circulation in one pair,
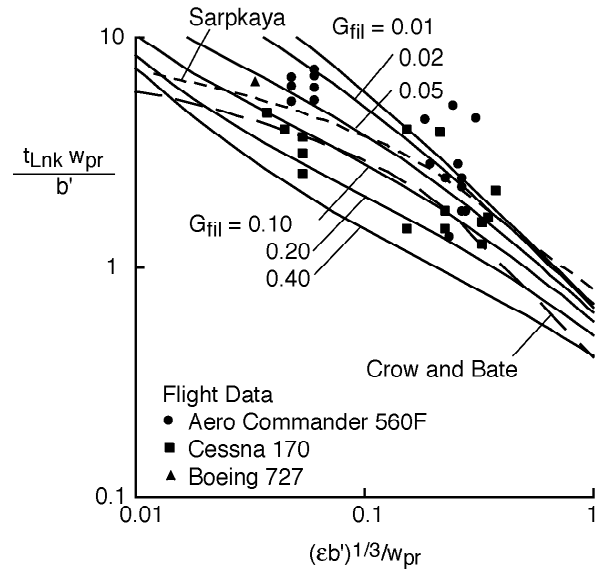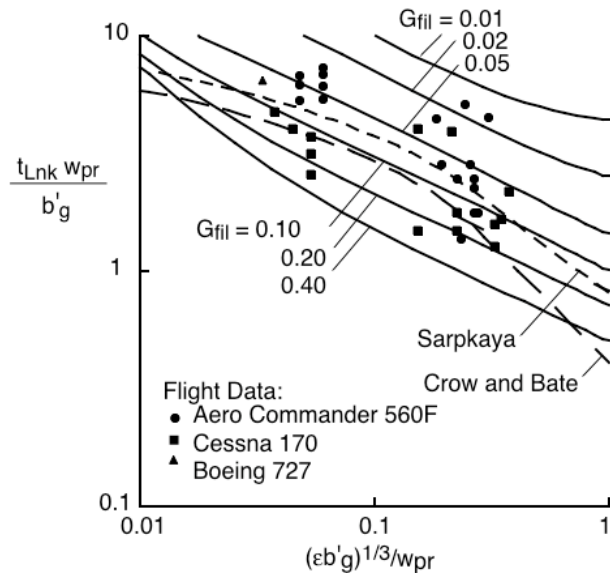
and to diffuse circulation in another nearby pair which does not link. Identification of vortex pairs where the circulation is diffusely distributed is usually not possible in the laboratory or in flight. The observations presented in the Appendix were all made at altitudes well above the ground plane,[22,31,32] because condensation of exhaust gases at those altitudes provides flow-field ice crystals for visualization that enables observations of wake dynamics. For these reasons, wake division is a possible explanation, even without knowledge of why or how the division occurs.

   The flight data points below the theoretical curve of Crow and Bate in Figs. 8 and 9, suggest that the vortex filaments in those cases contained more circulation than usually present in G_{ac} , which seems unreasonable. It is suggested, therefore, that the scatter in the flight data below the theoretical curve may be due to a mis-interpretation or mis-application of the measurement of the maximum perturbation velocities present in the atmospheric turbulence associated with those cases. Because the eddy-dissipation rate assumed by Crow and Bate[19] does sometimes not obey the Kolmogorov model, it may not be valid for some cases of atmospheric turbulence.[35,36,40-42] If true, the magnitudes of the disturbance velocities that initiate the long-wave instability may not have been correctly determined. Because the effective wave length of the disturbance velocities that initiate the long-wave instability are on the order of multiple wing spans, the time/distance profile of the disturbance velocities is more like gusts than like boundary-layer turbulence, which is the basis of turbulence models like that of Kolmogorov. Therefore, it is suggested that the use of instrumentation that measures, $|v'|_{max}$ and/or $|w'|_{max}$ for ε_{max} along the flight path of the wake-generating aircraft is more reliable than the methods used to determine the curves and data points in Figs. 7 and 8. Because effective wave lengths range from around 2 b' to 10 b', it is recommended that a parameter like ε_{max} be used to characterize the disturbance velocities, instead of an energy/frequency model. Such a procedure is also more likely to insure that the predictive process is based on shortest linking times, and not on a root-mean-squared value.

B. Linear Axes and Recommended Parameters.

   Figs. 7-9 retained the axis parameters used by Crow and Bate which employ which logarithmic scales to achieve continuity with previous research. However, when operations are underway at airports, it is recommended that linear scales, as shown in Fig. 10, be used on the graphs to present and analyze filament-linking times. Linear scales facilitate interpretation of the data and the location of acceptable and non-acceptable boundaries for wake-intrusion situations. It is also recommended that the graphical results being used have commonly used physical variables. As an example of convenience of interpretation, it is pointed out that when an often used aircraft with a 200 ft wingspan is on approach, its flight velocity is about 200 ft/s. The time-to-linking values, t_{Lnk}, shown in Fig, 10, are then in seconds, which is convenient for use by pilots and controllers. Furthermore, a value of $|w'|_{max}$ of 0.1 at the far right side of Fig. 10 would indicate maximum lateral and vertical gusts of 20

Fig.10 Velocity-based estimate for linking time plotted on linear scales recommended for applications.

ft/s in a turbulent/gusty atmosphere along the flight path of the aircraft. As indicated in Fig. 10, measurement of maximum disturbance velocities is recommended for wake-intrusion advisories. Reliability, consistency and ease of measurement need to be studied with flight experiments in order to determine the best way to measure atmospheric disturbance velocities to obtain a reliable value for the size of the safe zone indicated in Fig. 1.
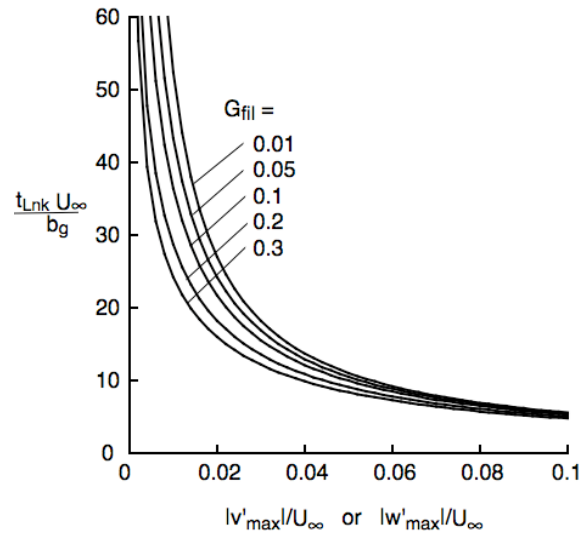
VIII. Conclusions

   It has long been known that the long-wave instability of a vortex pair is the aerodynamic mechanism that decomposes and spreads lift-generated vortex wakes faster than any other aerodynamic mechanism. As such, wake-avoidance methods require that the process be accurately represented theoretically and experimentally so that reliable predictions can be made of the wake-spreading rate as a function of the turbulence level in the atmosphere

where the vortex wake resides. This paper extends previous understanding of the characteristics of the long-wave instability to increase the reliability of formulations designed to predict the duration of the safe zone for aircraft executing nearly simultaneous landings on a set of closely-spaced parallel runways. Examination of available flight measurements indicate two reasons for the large amount of scatter in the time at which vortex pairs link across the spanwise distance between them to form irregularly-shaped loops of vortex filaments. The analysis first indicates that a value for the circulation content of the filaments based on the initial structure of the vortex pair is too large, because wake dynamics indicates that not all of the circulation shed by the aircraft wing goes into the filaments undergoing the long-wave instability. A second reason for the scatter in the flight measurements is believed to be caused by the method used to determine the magnitude of the turbulence or disturbance velocities in the atmosphere that initiate the long-wave instability. The method recommended previously for measurement of the turbulence level in the atmosphere is based on the entire spectrum of turbulence in the atmosphere, and not simply on the magnitude of the disturbance velocities in the wave-length range that initiates the long-wave instability. The complexity of such a measurement method, and its root-mean-squared characteristic, suggest that measurement of maximum disturbance velocities in the atmosphere is more reliable for the determination of wake-intrusion times, and may be easier to determine.

Appendix. Observations of Wake Division At Cruise Altitudes.

A. Pictures of Lift-Generated Wakes at Cruise altitudes.

The purpose of this appendix is to discuss the possibility that vortex pairs shed by aircraft may divide into two pairs of vortical (or vortex-type) regions. An aerodynamic mechanism consistently responsible for the division of one vortex pair into two pairs was not found. The reasons for a discussion of wake division in an Appendix is that both the analysis presented in the foregoing text and the observations of vortex wakes at cruise altitude have indicated that wakes divide. The observations indicate that the division process places an upper region of condensate (which appears to not have any organized vortex motions) and a lower region composed of vortex condensation cores (or filaments of small but finite diameter) that undergo the long-wave instability. It is estimated that the vortex condensation cores that go through the long-wave instability contain 40% or less of the initial circulation content of lift-generated vortices shed by the aircraft. In other words, the initial vortex structure not far behind the wake-generating aircraft divides into a vortex-core part with concentrated circulation, and a part with widely distributed circulation, which has no apparent organized structure, but may contain 60% or more of the original total circulation. Flow-field structures that behave in this way have been observed in photographs taken of condensation trails behind aircraft flying at cruise altitudes. The pictures presented here were taken at cruise altitudes because it is at those altitudes that condensation trails* frequently form behind subsonic transport aircraft.

Although a number of examples were photographed from the ground for preparation of an earlier paper,[22] the
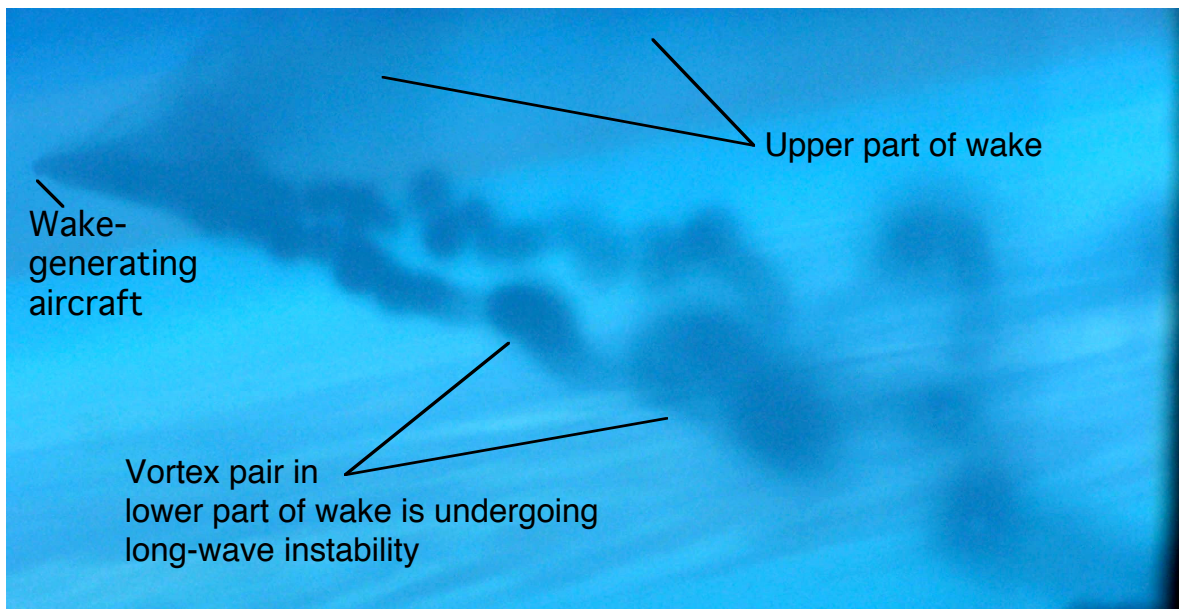

Fig. A1 Photograph taken from nearby aircraft of the condensation trail of a transport aircraft at cruise altitude. View from behind shows wake division into upper and lower parts. Upper part appears to not contain a pair of concentrated vortex cores, whereas lower part does contain a pair of intense vortex cores that are undergoing the long-wave instability. Photograph by A. Brown, National Research Council of Canada. Reproduced with permission. [31]

clearest example of wake separation is provided by Brown[31,32] (Fig. A1). The picture was taken by an aircraft flying near and into the wake of another aircraft to make measurements of wake velocities. The objective of the flight was to first determine wake structure for research and safety purposes, and then to identify and measure any potential hazard that the changing wake might pose to aircraft that accidentally penetrate the wake.[31,32] In the

---

* Condensation trails appear behind aircraft when they fly at cruise altitudes, because the atmosphere at those altitudes is often at temperatures below -40°F (or -40°C), and a relative humidity above 40%. These conditions cause the water vapor in engine exhaust gases to condense and freeze into ice crystals before they have time to evaporate or sublime. For this reason, exhaust condensate becomes a fluid marker of long duration that makes it possible to observe the dynamics of lift-generated vortex wakes over a wide range of conditions.[22,31,32]

American Institute of Aeronautics and Astronautics

photograph, the formation of two distinct regions of wake fluid indicate that the wake has divided into two regions. The lower part of the condensation trail contains a pair of condensation vortex cores that are in the early stages of the long-wave instability. The upper part appears to be a cloud of condensate without any organized structure, or presence of vortex cores. Also, a small non-condensate vertical distance appears to exist between the two parts of the wake. Brown[31,32] refers to the upper region as the jet-wake part of the wake, because it appears to consists primarily of engine exhaust, and the lower region as the vortex wake, because the two vortex cores in the photograph are clearly undergoing the long-wave instability.

The photographs in Fig. A2-A4 were taken at long range from the ground, and therefore do not reveal some pf the details of the flow field.[22] They do show that the condensation region shed by an aircraft first remains straight and then enlarges slowly for some time after being shed (Fig. A2). The initial single region of condensate-marked air space then divides or separates into an upper part and a lower part, but a significant condensate-free region
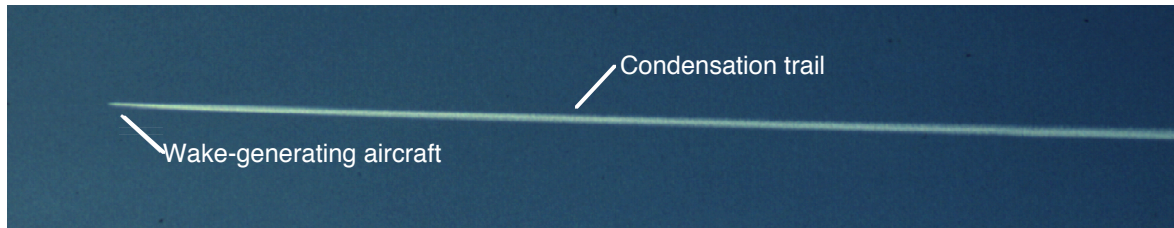

Fig. A2 Side view of beginning segment of condensation trail behind an aircraft before wake separation and linking appear.[22]

between them does not develop (Figs. A3 and A4). Other observations indicated that a pair of vortex cores do not become prominent until its presence is observed near the bottom of the condensation trail as the long-wave instability begins to develop. The development of the sinuous waves along the trails of the vortex cores becomes more apparent on the right side of Fig. A3, and appears to dominate the wake flow field in Fig. A4 because of the large amplitude of the waves and the vortex loops that are formed by the long-wave instability. The large appendages on the lower part of the condensation trail show how the long-wave instability causes the vortex pair to develop large across-wake displacements. On the right side of Fig. A4, the wake depth has increased by over a
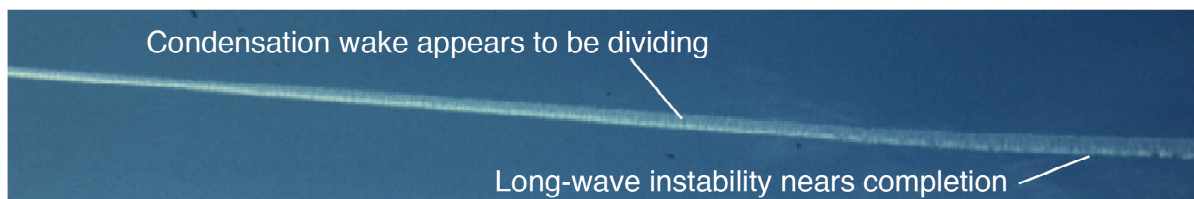

Fig. A3 About one-half minute after passage of wake-generating aircraft, same segment of condensation trail is separating into two parts. Striations around wake on left side of picture are shear-layer vortices from engine exhaust. Sinuous waves are also forming with vortex linking beginning in trail on right side of picture.[22]

factor of 5 due to the wake-spreading capability of the long-wave instability. Although not shown in Figs. A3 and A4, maximum wake displacements are about the same in both the lateral and vertical directions. Lateral
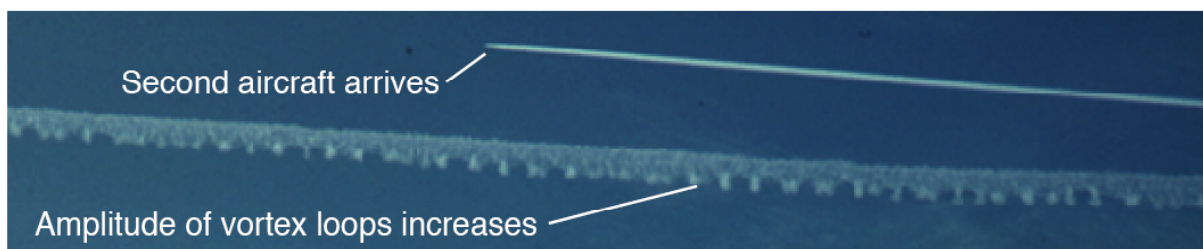

Fig. A4 Second aircraft begins flight above the first one. Lower wake from first aircraft is about one minute old and clearly exhibits loops formed by long-wave instability as condensate-marked air appendages hang down from upper region. Wake cross section has enlarged by over a factor of 5.[22]

displacements are shown in Fig. 2 in the body of the paper. During this time interval, the upper part of the condensate is dispersed by the large size of the loops of vortices formed by the long-wave instability because of the mixing that spreads the entire condensation trail. Throughout the dynamics of the long-wave instability, the top of the upper region exhibits large swirling regions similar to a large-scale turbulent fluid, but a clear sign of an organized or concentrated vortex pair never appears to be indicated.

Detailed pictures like those shown in Figs. A1-A4 are needed for the dynamics of vortex wakes of aircraft flying at approach and landing altitudes if the time-dependent structure of lift-generated wakes of aircraft in their approach configuration are to be adequately understood for optimum wake-avoidance procedures. Unfortunately, because fluid markers like the ice crystals at cruise altitude are not naturally available, some other types of flow visualization materials will be needed.

B. Wake Descent Velocity.

The curvature of the condensation trail (most obvious in Fig. A3 and A4) is caused by the slowing descent rate of the lift-generated wake as it ages and spreads. As the wake cross section enlarges due to spreading caused by turbulent diffusion and the long-wave instability, the downward momentum in the wake of the aircraft goes from being concentrated along the flight path to being spread over an increasingly larger cross-section of the wake, Fig. A4, the wake cross section appears to be larger by over 5 times across, and over 25 times in cross-sectional area. As a consequence, the downward velocity of the wake goes from around 5 ft/s (1.5 m/s) down to 1/25 times those values after the long-wave instability has gone to completion, which is a negligible velocity for all practical purposes.[33] The change in rate of descent of lift-generated wakes is estimated by first approximating its cross section with an elliptically-shaped region. The downward velocity of the wake may then be estimated by a theory based on the downward momentum induced in the wake by the lift force.[33] Therefore, if a value for wake breadth is available from observations[22] or from theoretical estimates, the downward velocity is roughly given by

$$w_{decomp}(t) \approx w_{pr} [B_{oval}/B_{decomp}(t)]^2 \qquad\qquad (A1)$$

where, $B_{oval} \approx 2.08 \ b'$ is the initial breadth of the oval-shaped wake, which is usually in a horizontal orientation. The quantity $B_{decomp}(t)$ is the breadth or horizontal extent of the decomposing wake. As vortex wakes age their breadth best represents the downward momentum in the wake due to the lift on the wake-generating wing. Therefore, as the wake spreads laterally, its descent velocity rapidly becomes smaller.

C. Possible Reasons for Wake Division.

When the classical analysis of the long-wave instability[18,19] was carried out, most aircraft were built with span loadings that were approximately elliptical. As a consequence, the vortex wakes shed by those aircraft had fairly concentrated vortical regions (or circulation) at the centers of the vortices that trail in their wake. The concentration of vorticity was then high enough near the wingtips of the generating aircraft that the two vortical regions, or vortices, could each be treated as a pair of vortex filaments which contain a large percentage of the circulation in the vortices. It was this approximation that enabled the development by Crow and Bate[19] of a single parameter relationship for the time required for the vortex pair to link in response to a measured intensity of ambient turbulence in the atmosphere where the wake is embedded.

Since that time, the development of high-speed computers has made it possible to optimize the design of the aircraft's lifting surfaces so that a given lift is produced for a minimum wing weight and efficiency, rather than for a given span. Such an optimization produces wings that have less drag, are stronger and weigh less, but have span lengths that are slightly larger than those designed by use of elliptically-loaded wings. Under such an optimization, span loadings are a combination of triangular and elliptical.[34] As a result, the circulation in the two vortices shed by the wings designed by weight optimization are now more evenly distributed across the wing trailing edge, and are not as highly concentrated near a wing tip. It is believed that this is a possible reason why the wakes shed by aircraft of recent vintage more often divide into two pairs of vortical regions, rather than remaining as one.

In order to examine how span loading on a wing affects the concentration of vorticity in trailing vortices, point-vortex distributions were used to represent the vortex wakes of 3 different span loadings on wings to study which produced vortex wakes that tended to divide into multiple pairs and which do not. Time-dependent calculations were first used to show that the vortex wakes of aircraft with elliptic loading do, as expected, roll up into a single pair of vortices, and remain so, with most of the circulation concentrated near their centers. A second computation examined triangular span loadings which showed that their vortex wakes do immediately divide about in half to produce two vortex pairs wherein the vortices on each side of the centerline orbit about each other. By use of the span loadings designed by Jones[34] for minimum wing-root bending moment (i.e., minimum weight), the wake first

begins as if wake division is about to occur, but the vortex sheet shed by the wing does eventually roll up into a single diffuse vortex pair. These simple simulations were not able to definitively show why vortex wakes divide. It may be that disturbances like jet exhaust plumes or turbulence also contribute to the cause of wake division.

XII. References

[1]Rossow, V. J., "Lift-Generated Vortex Wakes of Subsonic Transport Aircraft", *Progress in Aerospace Sciences*, Vol. 35, No. 6, Aug. 1999, pp. 507-660.

[2]Hinton, D. A., "Aircraft Vortex Spacing System (AVOSS) Conceptual Design", NASA TM 110184, Hampton, VA, Aug. 1995.

[3]Posluns, H., ed., *Proceedings of the International Wake Vortex Meeting*, Ottawa, Ontario, Canada, 2-4 Dec. 1997.

[4]Burnham, D. C., Hallock, J. N., and Greene, G. C., "Increasing Airport Capacity with Modified IFR Approach Procedures for Close-Spaced Parallel Runways", *Air Traffic Control Quarterly*, Vol. 9, No. 1, 2001, pp. 45-58.

[5]Rutishauser, D. K., and O'Connor, C. J., "Aircraft Wake Vortex Spacing System (AVOSS) Performance Update and Validation Study", NASA/TM-2001-211240, 2001..

[6]Hammer, J., "Case Study of Paired Approach Procedure to Closely Spaced Parallel Runways", *Air Traffic Control Quarterly*, Vol. 8, No. 3, 1999, pp. 223-252.

[7]Rossow, V. J., "Reduction of Uncertainties in Prediction of Wake-Vortex Locations", *AIAA Journal of Aircraft*, Vol. 39, No. 4, July-August 2002, pp. 587-596.

[8]Rossow, V. J., "Use of Individual Flight Corridors to Avoid Vortex Wakes", *AIAA Journal of Aircraft*, Vol. 40, No. 2, March-April 2003, pp. 225-231.

[9]Rossow, V. J., "Implementation of Individual Flight-Corridor Concept", AIAA-2003-6795, *AIAA 3rd Aviation, Technology, Integration, and Operations (ATIO) Forum* – An Aviation System for the 2nd Century of Flight, Denver, CO, Nov. 17-19, 2003.

[10]Rossow, V. J., Hardy, G. H., and Meyn, L. A., "Models of Wake-Vortex Spreading Mechanisms and Their Estimated Uncertainties", *AIAA 5th Aviation, Technology, Integration, and Operations (ATIO) Forum*, 26-28 Sept. 2005, Arlington, VA, AIAA 2005-7353.

[11]Rossow, V. J., "Classical Wing Theory and the Downward Velocity of Vortex Wakes", *AIAA Journal of Aircraft*, Vol. 43, No. 2, March-April 2006, pp. 381-385.

[12]Rossow, V. J., "Vortex-Free Flight Corridors for Aircraft Executing Compressed Landing Operations", *AIAA Journal of Aircraft*, Vol. 43, No. 5, Sept.-Oct. 2006, pp. 1424-1428.

[13]Rossow, V. J., Hardy, G. H., and Meyn, L. A., "Relationship Between Vortex Meander and Ambient Turbulence", *AIAA 6th Aviation, Technology, Integration, and Operations (ATIO) Forum*, 25-27 Sept. 2006, Witchita,KS, AIAA 2006-7811.

[14]Arkind, K. D., "Maximum Capacity Terminal Area Operations in 2022", AIAA 2003-6791, *AIAA 3rd Aviation, Technology, Integration, and Operations (ATIO) Forum* – An Aviation System for the 2nd Century of Flight, Denver, CO, Nov. 17-19, 2003.

[15]Miller, M. E., and, Dougherty, S. P. "Communication and the Future of Air Traffic Management", Paper No. 0-7803-8155-6/04, *2004 IEEE Aerospace Conference*, Big Sky Montana, March 6 -13, 2004.

[16]Hardy, G. H. and Lewis, E. K., "A Cockpit Display of Traffic Information for Closely Spaced Parallel Approaches", AIAA-2004-5106, *AIAA Guidance, Navigation and Control Conference and Exhibit*, 16-19, Providence, RI, August 2004.

[17]Powell, J. D., Jennings, C., and Holforty, W. L., "Use of ADS-B and Perspective Displays to Enhance Airport Capacity", *24th Digital Avionics Systems Conference*, Daytona Beach, FL, Paper No. 154, Session 2A, 3 Nov. 2005.

[18]Crow, S. C., "Stability Theory for a Pair of Trailing Vortices", *AIAA Journal*, Vol. 8, No. 12, Dec. 1970, pp 2172-9.

[19]Crow, S. C., and Bate, E. R., Jr., "Lifespan of Trailing Vortices in a Turbulent Atmosphere", *AIAA Journal of Aircraft, Vol.* 13, No. 7, July 1976, pp 476-482.

[20]Tombach, I. H., "Observations of Atmospheric Effects on Vortex Wake Behavior," *AIAA Journal of Aircraft*, Vol. 10, No. 11, Nov. 1973, pp. 641-647.

[21]Rossow, V. J., "Prospects for Destructive Self-Induced Interactions in a Vortex Pair", *AIAA Journal of Aircraft*, Vol. 24, No. 7, July 1987, pp. 433-440.

[22]Rossow, V. J., and James, K. D., "Overview of Wake-Vortex Hazards During Cruise", *AIAA Journal of Aircraft,* Vol. 37, No. 6, 2000, pp. 960-975.

[23]Liu, H.-T., and Srnsky, R. A., "Tow Tank Simulation of Vortex Wake Dynamics", Hallock, J. N., ed., *Proceedings of the Aircraft Wake Vortices Conference*-Vol.1 and 2, U. S. Dept. of Transportation, Federal Aviation Admin., DOT/FAA/SD-92/1.1, DOT-VNTSC-FAA-92-7.1, Washington, D. C., Oct. 29-31, 1991, pp. 32-1-26.

[24]Liu, H.-T., "Effects of Ambient Turbulence on the Decay of a Trailing Vortex Wake", *AIAA Journal of Aircraft*, Vol. 29, No. 2, March-April 1992, pp. 255-263.

[25]Sarpkaya, T., and Daly, J. J., "Effect of Ambient Turbulence on Trailing Vortices," *AIAA Journal of Aircraft*, Vol. 24, No. 6, June 1987, pp. 399-404.

[26]Sarpkaya, T., "Decay of Wake Vortices of Large Aircraft," *AIAA Journal of Aircraft*, Vol. 36, No. 9, Sept. 1998, pp. 1671--1679.

[27]Sarpkaya, T., "New Model for Vortex Decay in the Atmosphere," *AIAA Journal of Aircraft*, Vol. 37, No. 1, Jan.Feb. 2000, pp. 53-61.

[28]Sarpkaya, T., Robbins, R. E., and Delisi, D. P., "Wake-Vortex Eddy-Dissipation Model Predictions Compared with Observations," *AIAA Journal of Aircraft*, Vol. 38, No. 4, July-Aug. 2001, pp. 687-692.

[29]Delisi, D. P., "Laboratory Measurements of the Effect of Ambient Turbulence on Trailing Vortex Evolution," *44th AIAA Aerospace Sciences Meeting and Exhibition*, Reno, NV, Jan. 2006, AIAA 2006-1078.

[30]Delisi, D. P., Greene, G. C., Robins, R. E., "Aircraft Wake Vortex Core Size Measurements," 21st *AIAA Applied Aerodynamics Conference*, Orlando, FL, 23-26 June 2003, AIAA 2003-3811.

[31]Brown, A. P., "The Impact Upon Aircraft Airworthiness Design From Encounters with Discrete Vortices", AIAA 2006-229, *44th AIAA Aerospace Sciences Meeting and Exhibit,* Reno, NV, January 2006.

[32]Brown, A. P., and Bastian, M., "A Feasibility Study on the Inflight Measurement of Enroute Wake Vortex Characteristics", AIAA 2004-5366, *AIAA Atmospheric Flight Mechanics Conference*, Providence, RI, August 2004.

[33]Rossow, V. J., "Classical Wing Theory and the Downward Velocity of Vortex Wakes", *AIAA Journal of Aircraft*, Vol. 43, No.1, 2006, pp.1-6.

[34]Jones, R. T., "The Spanwise Distribution of Lift for Minimum Induced Drag of Wings Having a Given Lift and a Given Bending Moment", *NACA* Technical Note 2249, Dec. 1950; see also, "Collected Works of Robert T. Jones", NASA TM X-3334, Feb. 1976, pp. 539-554.

[35]Hinze, J. O., *Turbulence, An Introduction to Its Mechanism and Theory*, McGraw-Hill Book Co., Inc., 1959, pp. 180-190.

[36]Biswas, G., and Eswaran, V., *Turbulent Flows, Fundamentals, Experiments and Modeling*, Narosa Publishing House, New Delhi, India, 2002, pp. 44-58.

[37]Schlichting, H., *Boundary-Layer Theory*, McGraw-Hill Book Company, 1955, pp. 735-755.

[38]Zell, P. T., and Flack, K., "Performance and Test Section Flow Characteristics of the National Full-Scale Aerodynamics Complex 40- by 80-Foot Wind Tunnel", *NASA* TM 101065, Feb. 1989.

[39]Zell, P. T., "Performance and Test Section Flow Characteristics of the National Full-Scale Aerodynamics Complex 80- by 120-Foot Wind Tunnel", NASA TM 103920, Jan. 1993.

[40]McCready, P. B., Jr., "Turbulence Measurements by Sailplane," *Journal of Geophysical Research*, Vol. 67, No. 2, March 1962.

[41]McCready, P. B., Jr., Williamson, R. E., Berman, S. and Webster, A., "Operational Application of a Universal Turbulence Measuring System," *NASA* Contractor Report, NASA CR-62025, Nov. 1965.

[42]Department of Defense Handbook, *Flying Qualities of Piloted Aircraft*, MIL-STD-1797A, 28 June 1995, Appendix A, 4.9.2 Definition of atmospheric disturbance model form. Pp. 678-687.